SPAWAR
Systems Center
PACIFIC

Technical Report 2010
October 2012

Feasibility Study of a Nano-Communications Link Using Carbon Nanotube Antennas

John W. Rockway
Jeanne T. Quimby-Rockway
John D. Rockway
SSC Pacific

SSC Pacific
San Diego, CA 92152-5001

SSC Pacific
San Diego, California 92152-5001

J. J. Beel, CAPT, USN
Commanding Officer

C. A. Keeney
Executive Director

ADMINISTRATIVE INFORMATION

This report was prepared by the Electromagnetics Technology Branch of the SOS and Platform Design Division, Space and Naval Warfare Systems Center Pacific (SSC Pacific.)

Released by
M. Osburn, Head
Electromagnetics Technology Branch

Under authority of
J. McGee, Head
SOS and Platform Design Division

EXECUTIVE SUMMARY

This report details a feasibility study investigating the performance of a nano-communication system. The study is based on analyzing the suitability of carbon nanotube-based antennas to establish an effective communication link. A simulation has been developed that estimates the signal-to-noise ratio (SNR) between a carbon nanotube transmitter and its receiver separated across a free-space channel. The carbon nanotube antennas are modeled using a thin-wire approximation to the electric field integral equation and solved using the Method of Moments. In addition, the surface impedance on each wire is derived from a π-spatial tight binding model, which approximates the quantum conductive behavior of the carbon nanotube. To estimate the Total Channel Loss, the Linville method is used to determine the power delivered from the transmit antenna to the receiver. This simulation methodology is used to perform SNR calculations for a vertical carbon-nanotube dipole system in two different frequency bands (i.e., high GHz, optical). The performance of this nano-communication system is analyzed by conducting a trade-off study to determine the required input power necessary to establish an effective SNR.

CONTENTS

FIGURES

1. INTRODUCTION

Carbon nanotubes show excellent promise for nanoelectronic applications. Because of small size and distinct electrical properties, carbon nanotubes can be used to manufacture active device structures, such as single-electron transistors [1], or used as nano-sized, passive structures like vias and interconnects [2], [3] and [4]. In this report, the more recent application of exploiting the quasi-ballistic transport behavior of carbon nanotube for antenna applications is studied. As reported in References [5] and [6], when excited electromagnetically, a carbon nanotube radiates as a dipole antenna according to its electrical length. Since the sizes of carbon nanotubes are easily manufactured into micron and nano-sized lengths, the radiation from these dipoles can be tuned to desired frequencies in the high gigahertz (GHz) and optical frequency bands [8]−[10]. Research is continuing as to the suitability of carbon nanotubes as nano-antennas.

There have been several approaches to studying the electromagnetic properties of carbon nanotube antennas. Reference [5] developed a quantum conductivity model for armchair and zigzag carbon nanotubes and used the model to study the electromagnetic dynamics and surface wave propagation along the carbon nanotube. Reference [6] developed a transmission line model of a carbon nanotube antenna and calculated appropriate antenna parameters. In Reference [7], a finite element method was developed to analyze arrays of carbon nanotube antennas at terahertz frequencies. In References [8] through [10], Hanson modeled a carbon nanotube transmitting antenna as a thin-wire antenna. Its electromagnetic properties were then determined by solving a Hallén's integral equation using the Method of Moments. This approach was used to study the fundamental transmitting properties of carbon nanotubes in the high GHz [8], and at optical frequencies [9]. These approaches have principally focused on the transmitting properties of a carbon nanotube antenna. Currently, there are no reported studies that address the question of whether the small signal strengths that are being transmitted by the carbon nanotubes are sufficient to be received and effectively establish a communication link.

In order for a signal to be detected and received, there is a minimum signal-to-noise (SNR ratio that must be present in order for the transmit antenna to communicate effectively to a receiving antenna. One of the important findings of Hanson's work was that the efficiencies for carbon nanotube dipole antennas were reported to be very low (i.e., on the order of 10^{-4} to 10^{-6}) [8]−[10]. This means that less than .0001% of the power from the transmitter is actually being radiated. In contrast, a perfect conducting, half-wave dipole will typically have gains of approximately 2.15 dB and very high efficiencies. When compared to the perfect conducting, half-wave dipole antenna, carbon nanotube-based antennas are clearly poor transmitters. Carbon nanotube-based antennas require greater input power to overcome the inherent high resistance and ohmic losses of the carbon nanotube. However, large electric field strengths may not be required to sense, detect, or communicate at the nano-level. This issue is examined by quantifying the energy coupling between two carbon nanotube antennas.

The goal of this report is to calculate the SNR between a transmitter and receiver antenna system composed of two carbon nanotubes. For the purpose of this analysis, a communication link equation [10] is used to evaluate the SNR. The link equation is expressed as

$$\left[P_T - L_{T,mismatch}\right] + \left[D_T + \eta_T + D_R + \eta_R - L_P - L_{R,mismatch}\right] - N_R > SNR_{required} \quad (1)$$

All values in Equation (1) are in dB. P_T is the signal power from the transmitter. $L_{T,\,mismatch}$ is the signal power reflected from the transmit antenna because of the impedance mismatch between the transmitter and the transmit antenna.

The signal power delivered to the transmit antenna is $[P_T - L_{T,\,mismatch}]$. D_T and η_T are the directivity of the transmit antenna and the transmit antenna efficiency, respectively. Similarly, D_R and η_R are the directivity of the receive antenna and the receive antenna efficiency, respectively. L_{PROP} is the propagation loss between transmit and receive antennas. $L_{R,\,mismatch}$ is the signal power reflected from the receiver load because of the impedance mismatch between the receiver and the receive antenna. The Total Channel Loss between signal power from the transmitter and the signal power delivered to the receiver will be defined as

$$\text{Total Channel Loss} = D_T + \eta_T + D_R + \eta_R - L_{PROP} - L_{R,\,mismatch} \tag{2}$$

Finally, N_R is the receiver noise power. In order for a communication link to be established, the signal power at the receiver must be greater than the receiver noise power. The signal power at the receiver minus the receiver noise power must be greater than the required signal-to-noise, or $SNR_{required}$. The $SNR_{required}$ is determined by the properties of the communication channel and the type of modulation and demodulation being used.

A simulation is used to determine many of the link parameters in Equation (1). The basis for this simulation is the modeling of the electromagnetic field distribution using the thin-wire electric field integral equation [14]. The Method of Moments [13] is used to solve this integral equation. Since carbon nanotubes are nano-scale devices, the quantum conductive behavior of the carbon nanotube must be incorporated into the model. An approach, introduced by Hanson, is used where the surface impedance on the wire is modeled using Slepyan's π-spatial tight binding approximation [8]. This approximation provides an appropriate model for the quantum conductive behavior of the carbon nanotube. Once the field distribution has been calculated, the antenna parameters and signal strengths can then be determined and analyzed for the communication link. The electromagnetic simulation and communication link analysis were all performed using a modification of the computational electromagnetic code MININEC [18].

The link equation, Equation (1), will be evaluated for a vertically directed carbon nanotube dipole transmitter and receiver antenna. The two dipole antennas are separated across a free-space channel. The evaluation is performed at two distinct operating ranges, in the high GHz and optical frequency bands. The carbon nanotubes are assumed to be both single-walled, armchair carbon nanotubes. Based on this analysis, a trade-off study is performed to determine what input power is required to establish an effective SNR for a given antenna separation. Finally, a study is performed to improve the SNR of the communication link by increasing the directivity of the carbon nanotube antennas. A YAGI antenna is considered. This study is used is to estimate the efficacy of a carbon nanotube-based antenna communication system.

2. ELECTROMAGNETIC MODELING OF CARBON NANOTUBE ANTENNAS

2.1 ELECTRIC FIELD INTEGRAL EQUATION

Figure 1 shows a nanotube transmit dipole antenna and a nanotube receive dipole antenna. The transmit carbon nanotube is excited using a voltage source $\mathbf{E}^i(\mathbf{r}, \omega) = V_s$ at the operating frequency of $\omega = 2\pi f$. This excitation induces currents on the nanotube transmit dipole antenna. This current radiates outward to generate a scattered electric field $\mathbf{E}^s(\mathbf{r}, \omega)$, which excites and induces a current on the nanotube receive dipole antenna. The unknown current distribution $\mathbf{I}(\mathbf{r})$ induced on both the transmitter and receive carbon nanotubes are calculated. This electromagnetically coupled system is modeled using the thin-wire electric field integral equation. This integral equation is solved using the Method of Moments [13] for the current distribution induced on the carbon nanotubes. Once the currents have been determined, electromagnetic properties and antenna parameters can then be computed. The results can then be used to determine the performance of a nanotube dipole-based communication system.

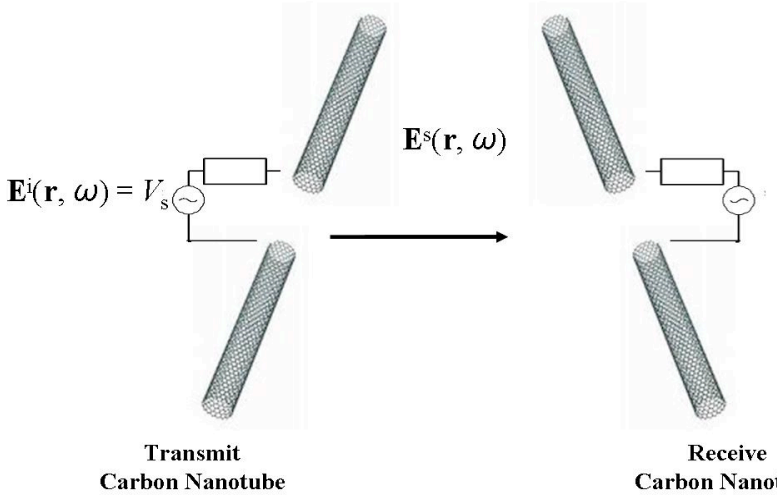

Figure 1. Communication system using carbon nanotube dipole antennas.

The electric field integral equation for the coupled antenna system is given by

$$\left[\mathbf{E}^i(\mathbf{r},\omega) + \mathbf{E}^s(\mathbf{r},\omega)\right]_{\tan} = Z_s \frac{\mathbf{I}(\mathbf{r})}{2\pi a(\mathbf{r})} \tag{3}$$

The scattered electric field $\mathbf{E}^s(\mathbf{r}, \omega)$ is expressed in terms of the mixed magnetic vector and electric scalar potentials as

$$\mathbf{E}^s(\mathbf{r},\omega) = -j\omega\mathbf{A}(\mathbf{r},\omega) - \nabla\Phi(\mathbf{r},\omega) \tag{4}$$

In free space, the vector and scalar potentials are defined as

$$\mathbf{A}(\mathbf{r},\omega) = \frac{\mu_o}{4\pi}\int_S \frac{\mathbf{I}(\mathbf{r}')}{2\pi a(\mathbf{r}')}\frac{e^{-jkR}}{R}dS' \tag{5}$$

and

$$\Phi(\mathbf{r},\omega) = -\frac{1}{j4\pi\omega\varepsilon_o}\int_S \nabla'_S \cdot \left(\frac{\mathbf{I}(\mathbf{r}')}{2\pi a(\mathbf{r}')}\right)\frac{e^{-jkR}}{R}dS' \tag{6}$$

where R = |**r** – **r**′| is the distance between the source and observation points. $k = \omega\sqrt{\mu_o\varepsilon_o}$ is the free-space wave number. $a(\mathbf{r})$ is the radius of the carbon nanotube and is assumed constant on each of the two carbon nanotubes. $\mathbf{I}(\mathbf{r})$ is the current vector directed along the wire axis. The magnitude of $\mathbf{I}(\mathbf{r})$ is the total current on the wire surface *S*. The quantities μ_o and ε_o are the permeability and permittivity of free space, respectively. By combining Equations (3) through (6), the Electric Field Integral Equation (EFIE) for a carbon nanotube-based antenna is formulated to be

$$Z_s\frac{\mathbf{I}(\mathbf{r})}{2\pi a(\mathbf{r})} + \frac{\mu_o}{4\pi}\int_S \frac{\mathbf{I}(\mathbf{r}')}{2\pi a(\mathbf{r}')}\frac{e^{-jkR}}{R}dS' + \frac{1}{j4\pi\omega\varepsilon_o}\int_S \nabla'_S \cdot \left(\frac{\mathbf{I}(\mathbf{r}')}{2\pi a(\mathbf{r}')}\right)\frac{e^{-jkR}}{R}dS' = \mathbf{E}^i_{\tan}(\mathbf{r},\omega) \tag{7}$$

2.2 SURFACE IMPEDANCE BASED ON QUANTUM CONDUCTIVE BEHAVIOR

The surface impedance, Z_s, is defined on the wire, which takes into account the quantum conductive behavior. The surface impedance Z_s in Equation (7) is derived based on Slepyan's π-spatial tight binding approximation [5]. Using this approximation, the surface impedance Z_s per unit length is given by

$$Z_s = \frac{1}{2\pi a(\boldsymbol{r})\sigma_{CN}} \tag{8}$$

where σ_{CN} is the conductivity. The radius $a(\boldsymbol{r})$ of the carbon nanotube is given by Equation (8),

$$a(\mathbf{r}) = \frac{\sqrt{3}}{2\pi}b\sqrt{m^2+mn+n^2} \tag{9}$$

where (*m*, *n*) is the chiral pattern and *b* is the interatomic distance in grapheme, which is approximately 2.91 nm. For the purpose of this analysis, armchair carbon nanotubes will be considered. For armchair carbon nanotubes *m* = *n*. Assuming a small radii approximation, the conductance is given by the following formula [5,12]

$$\sigma_{CN} = \frac{je^2\omega}{\pi^2 \mathrm{h} a}\left(\frac{-3\gamma_o b/\mathrm{h}}{\omega(\omega - j\nu)} + 2\sum_{s=1}^{m}\int_{-2\pi\mathrm{h}/\sqrt{3}}^{2\pi\mathrm{h}/\sqrt{3}} E_c\left|R_{vc}\right|^2\frac{(F_c - F_v)}{\mathrm{h}^2\omega(\omega - j\nu) - 4E_c^2}dp_z\right) \tag{10}$$

$F_{c,v}$, $E_{c,\mathrm{v}}$, and $R_{c,v}$ are given by the expressions

$$F_{c,v} = (1 + e^{E_{c,v}/(k_bT)})^{-1}$$

$$E_{c,v}(p_z,s) = \pm\gamma_o\sqrt{1+4\cos(\pi s/m)\cos(dp_z/\sqrt{3})+4\cos^2(dp_z/\sqrt{3})}$$

and

$$R_{vc}(p_z,s) = -\frac{\sqrt{3}b\gamma_o^2}{2E_c^2(p_z,s)}\sin(dp_z/\sqrt{3})\sin(\pi s/m)$$

In these expressions, e is the charge of the electron. T is the temperature, $v = 1/\tau$ is the relaxation frequency, and $d = 3b/2\hbar$ is the quasi-momentum of the electron's conductance in the z-direction.

In Figure 2, the quantum conductivity is plotted for armchair nanotubes of radii a = 2.71 nm (m = 40) and a = 0.678 nm (m = 10) at the high GHz frequency band. In Figure 3, the quantum conductivity is plotted for armchair nanotubes of radii a = 2.71 nm (m = 40) and a = 0.678 nm (m = 10) at optical frequencies. At optical frequencies, there are resonant bands in the conductivity caused by optical inter-band transitions found in the second term of Equation(10). The high GHz frequency band is defined as 100 to 700 GHz. In this band τ = 3.0ps. The optical frequency band is defined as 400 to 750 THz. In this band, τ = .01ps. For both of these frequency bands, the temperature, T, is 295 degrees Kelvin (K) and γ_o = 3.03eV.

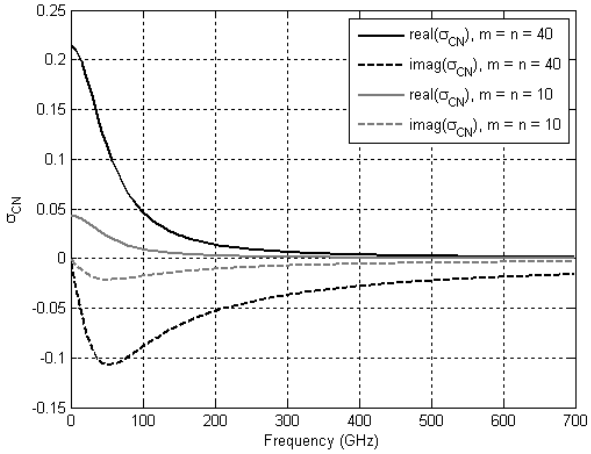

Figure 2. Quantum conductivity for high GHz of 100 to 700 GHz.

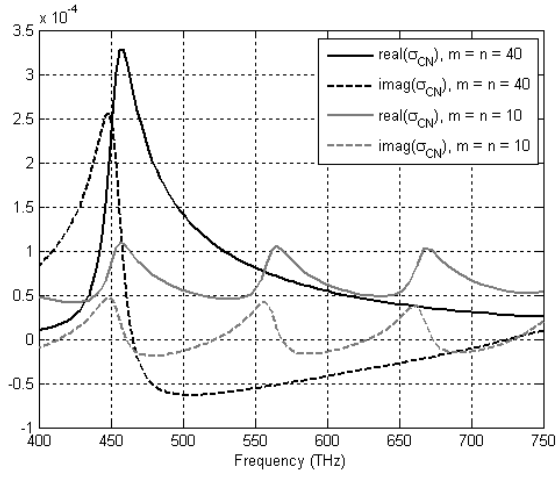

Figure 3. Quantum conductivity for optical frequencies of 400 to 750 THz.

Figure 4 and Figure 5 show the calculations for the surface impedance resistance (solid) and reactance (dash) for a carbon nanotube at optical frequencies (400–750 THz) and at the high GHz (100–700 GHz). The calculations are for two different radii, $a(\boldsymbol{r})$ = 2.71nm ($m = n = 40$) in black and $a(\boldsymbol{r})$ = 0.678nm ($m = n = 10$) in gray. At the high GHz of Figure 4, the quantum conductance model only depends on the first term in Equation (10). At these lower frequencies, the surface impedance does not depend on the radius of the carbon nanotube. Again, at optical frequencies of Figure 5, the ringing in the impedances is caused by optical inter-band transitions.

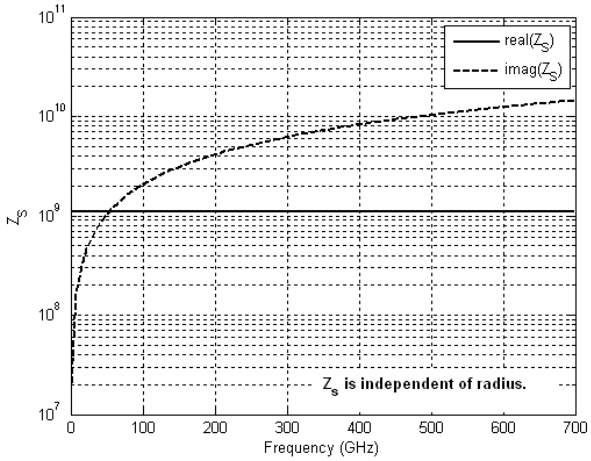

Figure 4. Surface impedance for high GHz of 100 to 700 GHz.

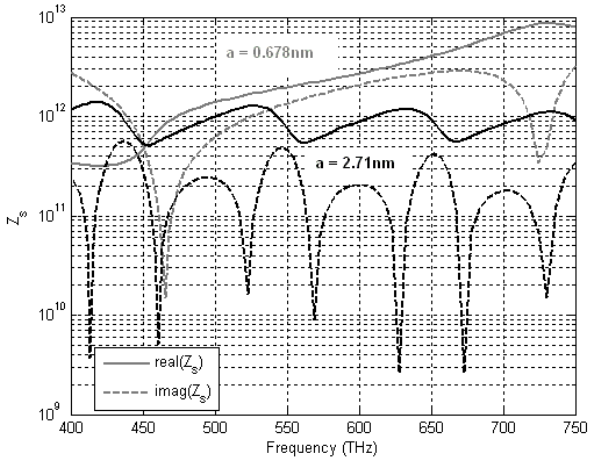

Figure 5. Surface impedance for optical frequencies of 400 to 750 THz.

3. THIN-WIRE METHOD OF MOMENTS

A thin-wire Method of Moments is used to numerically solve the EFIE in Equation (7) by transforming the integral equation into a linear system of equations. The carbon nanotube is first discretized into thin-wire segments of equal radii for each antenna. The unknown surface current across each wire segment is expanded in space using linear RWG wire basis function as

$$\mathbf{I}(\mathbf{r}) = \sum_{n=1}^{N} I_n \, \mathbf{\Lambda}_n(\mathbf{r}) \tag{11}$$

where I_n is the nth unknown current coefficient and $\mathbf{\Lambda}_n(\mathbf{r})$ is a basis function defined on the wire segments [14]. Referring to the geometry in Figure 6, the basis functions are defined on a wire segment as

$$\mathbf{\Lambda}_1(\mathbf{r}) = \frac{\xi_2 \mathbf{l}_1}{\mathrm{J}} \quad \text{and} \quad \mathbf{\Lambda}_2(\mathbf{r}) = \frac{\xi_1 \mathbf{l}_2}{\mathrm{J}} \tag{12}$$

The quantities ξ_1 and ξ_2 are the normalized coordinates of a wire segment, as shown in Figure 6, and are related by $\xi_2 + \xi_1 = 1, \xi_1 \in (0,1)$. The Jacobian ϑ is given by $\mathrm{J} = \left|\mathbf{l}^i\right|$ for a wire segment. The unitary basis vectors are

$$\mathbf{l}^i = \frac{d\mathbf{r}}{d\xi_i} \tag{13}$$

The tangent vectors for a wire segment are defined in terms of these vectors as $\mathbf{l}_2 = -\mathbf{l}_1 = \mathbf{l}^1$. Also, the divergence of the wire basis functions is given by

$$\nabla \cdot \mathbf{\Lambda}_n(\mathbf{r}) = \frac{1}{\mathrm{J}} \tag{14}$$

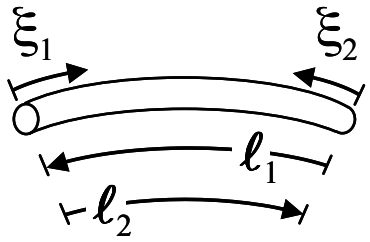

Figure 6. Element tangent to a curved wire segment.

Inserting Equation (11) into Equations (5) and (6) yields expressions that are written in terms of sums of partial potentials as

$$\mathbf{A}(\mathbf{r}) = \mu \sum_{n=1}^{N} I_n \int_{\sigma} \mathbf{\Lambda}_n(\mathbf{r}') K(\mathbf{r}, \mathbf{r}') d\sigma' \tag{15}$$

and

$$\Phi(\mathbf{r}) = \frac{-1}{j\omega\varepsilon}\sum_{n=1}^{N} I_n \int_{\sigma} \nabla'_S \cdot \mathbf{\Lambda}_n(\mathbf{r}') K(\mathbf{r},\mathbf{r}')\, d\sigma' \tag{16}$$

where the Green's function kernel is given by

$$K(\mathbf{r},\mathbf{r}') = \frac{1}{2\pi}\int_{-\pi}^{\pi} \frac{e^{-jkR}}{4\pi R} d\phi' \tag{17}$$

The substitution $dS' = a(\mathbf{r}')d\phi' d\sigma'$ is made, where dσ' is a differential arc length along the wire axis σ and $d\phi'$ is an angle differential measured about the wire circumference.

The vector $\mathbf{r}'$ in Equations (15) through (17) is reinterpreted as a vector to a point on the wire axis. This means that R is no longer $|\mathbf{r} - \mathbf{r}'|$, but is the distance from $\mathbf{r}$ to a point on the wire's surface with its circular cross section centered at $\mathbf{r}'$. Also, note that geometrical complexities such as bends, radii discontinuities, and junctions that can arise at wire segment endpoints are ignored; it is merely assumed that total current is continuous (or, equivalently, that Kirchhoff's current law is satisfied at a junction). There are no issues with using Equations (15) through (17) when the source and observation points are not close. However, when the observation point approaches the source point, the wire kernel becomes singular. In the past, the singular part was extracted in some way and evaluated analytically. With the recent transformation presented in References [14] and [15], singularity extraction is no longer needed since the inner integral's integrand is smoothed by variable transformations, whereas the logarithmically singular outer integral may be integrated numerically using the scheme described in Reference [15].

Next, a suitable testing scheme must be adopted. In this formulation, standard Galerkin testing functions are used in space, evaluated via a higher-order Gaussian rule. Applying Galerkin testing to the EFIE in Equation (7) yields the following linear system of equations,

$$\begin{aligned} &Z_s \int_S \frac{\mathbf{\Lambda}_m(\mathbf{r}) \cdot \mathbf{I}(\mathbf{r})}{2\pi a(\mathbf{r})} dS + \frac{\mu_o}{4\pi}\int_S\int_{S'} \frac{\mathbf{\Lambda}_m(\mathbf{r}) \cdot \mathbf{\Lambda}_n(\mathbf{r}')}{2\pi a(\mathbf{r}')} \frac{e^{-jkR}}{R} dS' dS \\ &+ \frac{1}{j4\pi\omega\varepsilon_o}\int_S\int_{S'} \frac{\nabla_S \cdot \mathbf{\Lambda}_m(\mathbf{r}) \nabla'_S \cdot \mathbf{I}(\mathbf{r}')}{2\pi a(\mathbf{r}')} \frac{e^{-jkR}}{R} dS' dS = \int_S \mathbf{\Lambda}_m(\mathbf{r}) \cdot \mathbf{E}^i_{\tan}(\mathbf{r}) dS, \quad m = 1,2,\text{K}\ ,N \end{aligned} \tag{18}$$

Finally, the partial potentials of Equations (15) through (17) are substituted into the Galerkin tested EFIE given by Equation (18). This yields the following linear system of equations,

$$\boldsymbol{Z}_{m,n}\boldsymbol{I}_n = \boldsymbol{V}_m, \quad m = 1,2,\text{K}\ ,N \tag{19}$$

which can be solved to determine the unknown current coefficients $\boldsymbol{I}_n$ located at the nodes between two wire segments making up each antenna. The matrix $\boldsymbol{Z}_{m,n}$ in Equation (19) is an N x N system of equations given by

$$\begin{aligned} \boldsymbol{Z}_{m,n} = {} & Z_s \int_S \frac{\mathbf{\Lambda}_m(\mathbf{r}) \cdot \mathbf{\Lambda}_n(\mathbf{r})}{2\pi a(\mathbf{r}')} dS + \frac{\mu}{4\pi}\int_S\int_{S'} \frac{\mathbf{\Lambda}_m(\mathbf{r}) \cdot \mathbf{\Lambda}_n(\mathbf{r}')}{2\pi a(\mathbf{r}') R} \frac{e^{-jkR}}{R} dS' dS \\ &+ \frac{1}{4\pi\varepsilon}\int_S\int_{S'} \frac{\nabla_S \cdot \mathbf{\Lambda}_m(\mathbf{r}) \nabla'_S \cdot \mathbf{\Lambda}_n(\mathbf{r}')}{2\pi a(\mathbf{r}') R} \frac{e^{-jkR}}{R} dS' dS, \quad m,n = 1,2,\text{K}\ ,N \end{aligned} \tag{20}$$

The right-hand side voltage $\boldsymbol{V}_m$ in Equation (18) is used to excite and is written as

$$V_m = \int_S \mathbf{\Lambda}_m(\mathbf{r}) \cdot \mathbf{E}^i(\mathbf{r})\, dS \tag{21}$$

For this analysis, the transmit antenna is excited using a voltage delta-gap generator source. In this case, the wire segments attached to a current node (junction) m can be thought of as separated by a gap across which the voltage $\boldsymbol{V}_m$ is specified.

4. FUNDAMENTAL ANTENNA PROPERTIES OF CARBON NANOTUBES

4.1 IMPEDANCE

The impedance of a nanotube transmit dipole antenna is shown in Figure 7. The half-length of the dipole antenna is 10 μm. The radius is 2.71 nm. This radius corresponds to an armchair carbon nanotube where m = n = 40. The resistance varies from approximately 10 to 140 kilo-ohms (i.e., thousands of ohms). The reactance varies from -80 to 50 kilo-ohms.

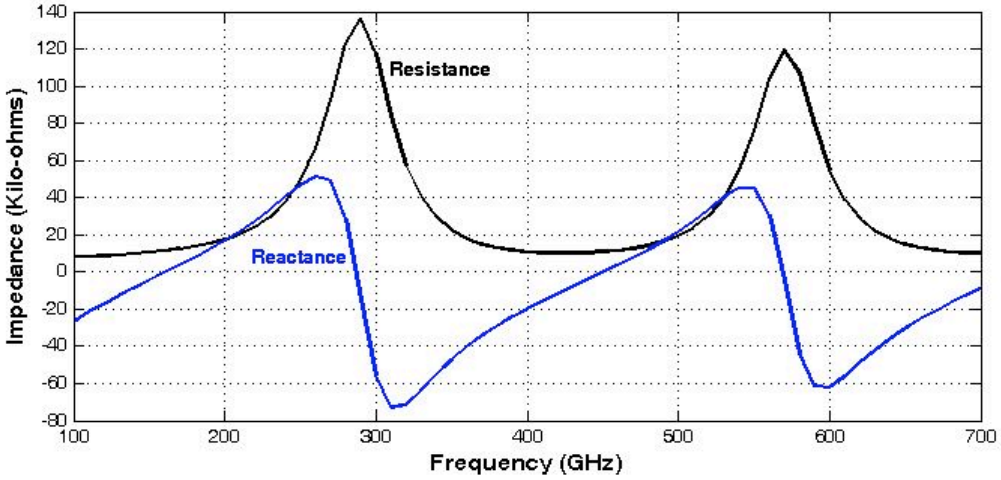

Figure 7. Impedance, high GHz.

4.2 FAR-FIELD RADIATION PATTERN

Once the induced currents on the carbon nanotubes antennas have been computed, the electromagnetic properties can be analyzed. The far-field electric field is approximated as

$$\mathrm{E}(R) = \frac{jk\eta}{4\pi}\frac{e^{-jkR}}{R}\int\left[\boldsymbol{k}\,\mathrm{g}\boldsymbol{I}(s)\boldsymbol{k} - \boldsymbol{I}(s)\right]e^{jk\,\mathrm{g}\,\boldsymbol{r}}\,dS \tag{22}$$

where $\boldsymbol{k}$ = (cosθ cosφ) **x** + (cosθ sinφ) **y** + (sinφ) **z** is the wave vector. $\eta = \sqrt{\mu_o/\varepsilon_o}$ is the free-space impedance. The vector R is the range vector from the current on the carbon nanotube wire to the far-field observation point. The integral is evaluated in closed form over each straight wire segment. The total far-field radiation pattern is then the sum of the contributions from all of the wire segments. Based on the far-field electric field calculation, the radiation pattern of the antenna is given by

$$P(\theta,\varphi) = \frac{1}{2}R^2\,\mathrm{Re}\left[\boldsymbol{E}\times\boldsymbol{H}\right] = \frac{R^2}{2\eta}\boldsymbol{E}\,\mathrm{g}\boldsymbol{E}^* \tag{23}$$

In Figure 8, the current distribution on a carbon nanotube dipole antenna is plotted at 200, 400, and 600 GHz. Again, the half-length of the dipole antenna is 10 μm and has a radius of 2.71 nm ($m = n =$ 40). Figure 9 shows the corresponding far-field radiation pattern for the dipole at these frequencies. All of the far-field patterns of Figure 9 show the classic sin (θ) pattern distribution of the small dipole.

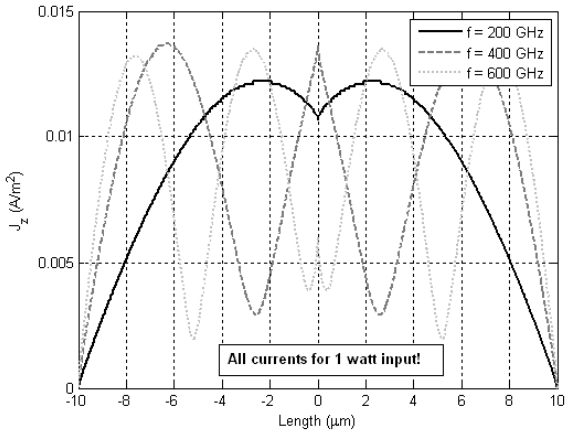

Figure 8. Current distribution, 10-μm half-length dipole antenna of radius of 2.71 nm.

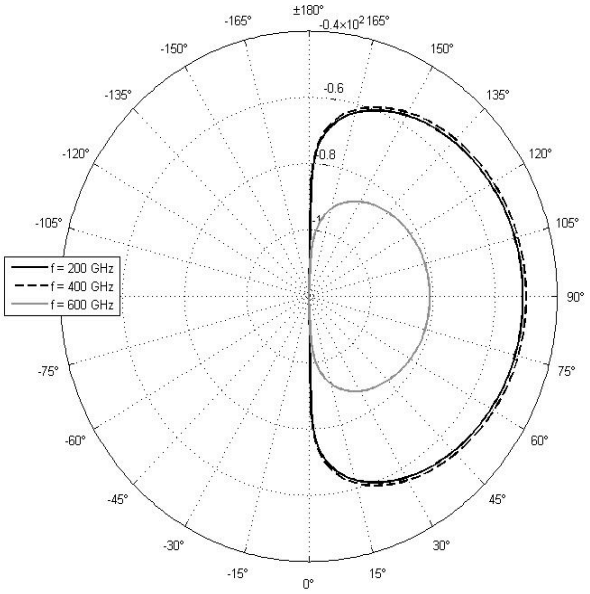

Figure 9. Far-field pattern, 10-μm half-length dipole antenna of radius of 2.71 nm.

The three-dimensional radiation pattern of the dipole at 200 GHz is shown in Figure 10.

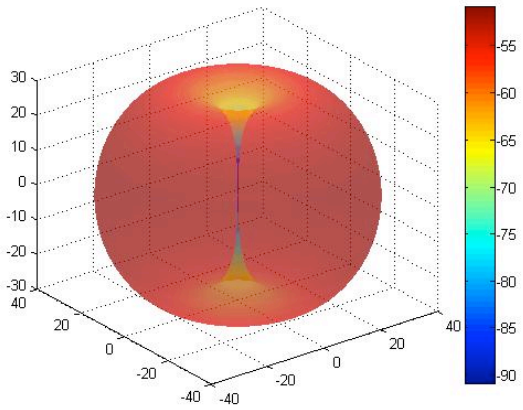

Figure 10. 3-D far-field pattern, 10-μm half-length dipole antenna of radius of 2.71 nm.

4.3 ELECTRIC NEAR FIELD

To provide better understanding of the magnitude of field strengths, the electric near fields in the vicinity of the antenna are simulated. The electric near fields can be determined from the current distribution by using the virtual dipole method [17]. To determine the electric field at a given point in the near field, a small virtual thin-wire dipole is placed at the point with its axis parallel to the appropriate vector component. The open-circuit voltage at the near-field point can be calculated from knowledge of the calculated current distribution and the mutual impedance between the carbon nanotube antenna and the virtual dipole. In other words,

$$V_d = \sum_{i=1}^{N} Z_{di} I_i \tag{24}$$

The virtual dipole is open-circuited, and V_d is the open-circuit voltage. I_i designates the computed currents on the wire structure. Z_{di} designates the mutual impedances between the wire structure and the virtual dipole. The mutual impedances are calculated from the Method of Moments. The electric field strength along the direction of the virtual dipole of length L_d is

$$\mathrm{E_d} = (\mathrm{V_d} / \mathrm{L_d})$$

The equation is evaluated once for each electric field component in the x, y, and z directions at the near-field point of interest. The virtual dipole length is .01 of the shortest segment length in the antenna segmentation.

The three electric field vector components, E_x, E_y, and E_z, are calculated as real and imaginary terms, from which the magnitude and phase are determined. The average value of the electric field is defined by $E_{ave} = |\boldsymbol{E}|$. The maximum or peak electric field is [17]

$$E_{peak} = \left[\frac{1}{2}(E_x{}^2 + E_y{}^2 + E_z{}^2) + \frac{1}{2}(A^2 + B^2)^{1/2} \right]^{1/2} \tag{25}$$

where

$$A = E_x^2 \cos(2\theta_x) + E_y^2 \cos(2\theta_y) + E_z^2 \cos(2\theta_z)$$

and

$$B = E_x^2 \sin(2\theta_x) + E_y^2 \sin(2\theta_y) + E_z^2 \sin(2\theta_z)$$

and where θ_x, θ_y, and θ_z are the phase angles for the corresponding field components.

In Figure 11 and Figure 12, the electric near field (x and z-components) of the 10-µm half-length nanotube dipole antenna and radius of 2.71 nm are shown. The dipole has been excited by 1 watt of power at 200 GHz.

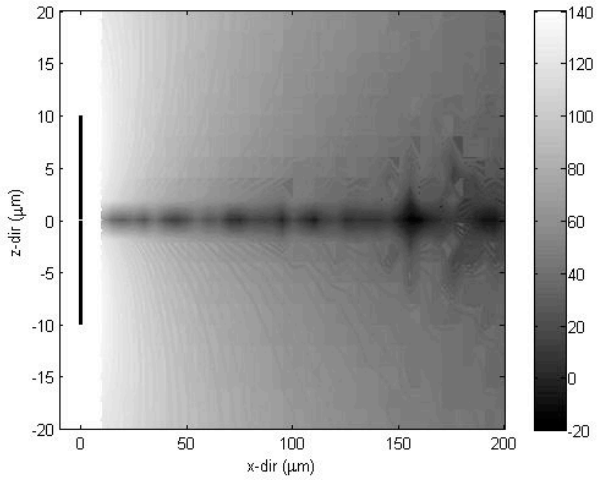

Figure 11. Electric near field E_x in dB, 10-µm half-length dipole antenna of radius of 2.71 nm.

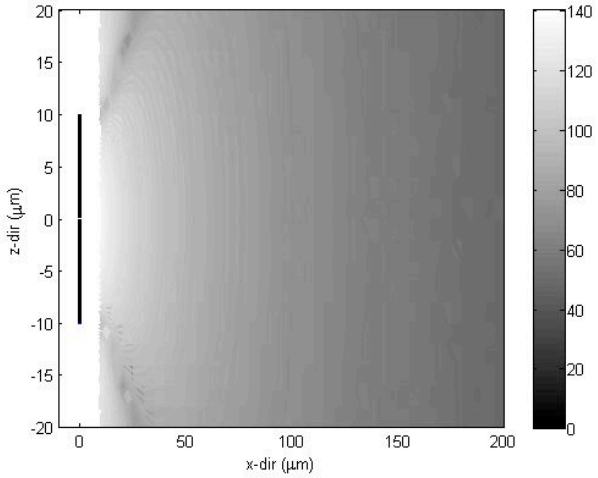

Figure 12. Electric near field E_z in dB, 10-µm half-length dipole antenna of radius of 2.71 nm.

4.4 EFFICIENCY

There are two methods for calculating the efficiency of a transmitting antenna structure. In the first method, the far-field power gain is calculated. The far-field power gain, in a given direction in spherical coordinates, is

$$G_{db}(\theta,\varphi) = 10\log_{10}\left[\frac{4\pi P(\theta,\varphi)}{P_{in}}\right] \tag{26}$$

where $G_{db}(\theta, \varphi)$ is the power radiated per unit steradian in the angular directions θ and φ. P_{in} is the total input power to the antenna calculated from the applied voltages V_s and the corresponding feed point currents I^*_s as

$$P_{in} = \mathrm{Re}(V_s I_s^*)/2 \tag{27}$$

Directive gain of a transmit antenna is the power gain divided by the efficiency of the antenna, or

$$D_{dB} = G_{dB} - \eta_{dB} \tag{28}$$

where η_{dB} is the efficiency in dB. The directive gain of a small antenna is 1.77 dB. The difference between this directive gain and the calculated power gain would be the efficiency.

In the second method, the ohmic power losses on the antenna structure can be calculated. The ohmic power loss is calculated from the currents of Equation (7) multiplied by the real part of the surface impedance, using

$$P_{ohmic} = 1/2\,|I|^2\,\mathrm{Re}(Z_{in}) \tag{29}$$

The input impedance of a carbon nanotube antenna is given by $Z_{in} = V_s / I_s$. The efficiency is then the radiated power, or the input power minus the ohmic power loss divided by the input power, or

$$\eta = \frac{P_{in} - P_{loss}}{P_{in}} \tag{30}$$

The two methods of analysis yielded similar efficiency values.

4.5 IMPEDANCE MISMATCH LOSS

Another loss is associated with the reflected power back to the transmitter because of impedance matching between the antenna impedance and the internal impedance of the transmitter. This mismatch loss reduces the power delivered to the transmit antenna. When a source is terminated with an antenna with an impedance of Z_{AT}, that is not equal to the internal impedance of the transmitter or source, Z_T, not all of the power is delivered to the antenna. This reflected power results in a mismatch loss of

$$L_{Tmismatch} = -20\log\left[\left|\frac{Z_{AT} - Z_T}{Z_{AT} + Z_T}\right|\right] \tag{31}$$

The input impedance is the source voltage divided by the current flowing at the source. For the purpose of this analysis, Z_T = 12,900 ohms. This impedance value is based on the nanoscale, dc electron transport [6]. A similar mismatch can be defined for the mismatch between the receive antenna impedance and the represented load of the receiver. This receive mismatch loss is

$$L_{Rmismatch} = -20\log\left[\left|\frac{Z_{AR} - Z_R}{Z_{AR} + Z_R}\right|\right] \tag{32}$$

4.6 RECEIVER NOISE POWER

Finally, for the purpose of this analysis, it is assumed that the receiver noise power is generated in the receiver itself. The contribution of external noise is minimal. The receiver noise power, N_R, is given by

$$N_R = kT_RB \tag{33}$$

where k is Boltzmann's constant. T_R is the receive system temperature and B is the receiver bandwidth. The receive noise temperature is usually determined from the Noise Figure in dB, NF_{dB}, of the receiver and the ambient temperature, 290 degrees Kelvin. The receive system temperature can be determined from

$$T_R = 290\left[10^{\left(\frac{NF_{dB}}{10}\right)} - 1\right] \tag{34}$$

4.7 TOTAL CHANNEL LOSS

In Equation (2), the Total Channel Loss was defined as $[D_T + \eta_T + D_R + \eta_R - L_{PROP} - L_{R,\,mismatch}]$. Rather than calculating each parameter in the Total Channel Loss, it is possible to calculate the Total Channel Loss directly using the Linville method [11].

The first step is to calculate the admittance parameters for the transmitter and receiver antenna system. Any two antennas can be treated as a two-port network, where terminals 1-1' would be the feed point of the first antenna and the terminals 2-2' would be the feed point of the second antenna. The two-port network equations can be written as

$$\begin{bmatrix} I_1 \\ I_2 \end{bmatrix} = \begin{bmatrix} Y_{11} & Y_{12} \\ Y_{21} & Y_{22} \end{bmatrix} \begin{bmatrix} V_1 \\ V_2 \end{bmatrix} \tag{35}$$

These admittance parameters are defined by the following relations

$$Y_{11} = \left.\frac{I_1}{V_1}\right|_{V_2=0}, \; Y_{12} = \left.\frac{I_1}{V_2}\right|_{V_1=0}, \; Y_{21} = \left.\frac{I_2}{V_1}\right|_{V_2=0}, \; Y_{22} = \left.\frac{I_2}{V_2}\right|_{V_1=0}$$

where V_1 and V_2 equal zero implies that the terminals associated with these voltages are short-circuited. The current calculation is used to find the admittance parameters. The feed point of one antenna is excited, and the feed point of the second antenna is short-circuited. The calculated currents are used to determine Y_{11}, Y_{12}, Y_{21}, and Y_{22}. Once the admittance parameters have been found, the Total Channel Loss can be calculated for arbitrary receiver loads.

To evaluate the maximum power transfer between the transmitter and the power received at the receiver or minimum Total Channel Loss, the input and output power must be determined. Given an unknown load on the receive antenna, the output power is determined by

$$P_{out} = \left|V_R\right|^2 \mathrm{Re}\left[Y_{load}\right] \tag{36}$$

where V_R is the output voltage on the receive load, and Re [Y_{load}] is the real part of the receive load admittance Y_{load}. Similarly, the input power can be calculated by

$$P_{in} = \left|V_T\right|^2 \mathrm{Re}\left[Y_{in}\right] \tag{37}$$

where V_T is the input voltage on the transmit antenna. Re [Y_{in}] is the real part of the input admittance of the transmit antenna port. Taking the ratio of Equations (36) and (37), a channel gain can be defined as

$$G_{Channel} = \frac{P_{out}}{P_{in}} = \frac{\mathrm{Re}\left[Y_{load}\right]}{\mathrm{Re}\left[Y_{in}\right]}\left|\frac{V_R}{V_T}\right|^2 \tag{38}$$

This ratio is dependent on the input admittance Y_{in} given by

$$Y_{in} = Y_{TT} - \frac{Y_{RT}Y_{TR}}{Y_{load} + Y_{RR}} \tag{39}$$

The two-port admittance parameters can then be used also to find the output to input voltage ratio, V_R / V_T, as

$$\left|\frac{V_R}{V_T}\right| = \left|\frac{Y_{RT}Y_{TR}}{Y_{load} + Y_{RR}}\right| \tag{40}$$

Substituting Equations (39) and (40) into Equation (38), the channel gain becomes

$$G_{Channel} = \frac{\mathrm{Re}\left[Y_{load}\right]}{\mathrm{Re}\left[Y_{in}\right]}\left|\frac{Y_{RT}Y_{TR}}{Y_{load} + Y_{RR}}\right| \tag{41}$$

In order to minimize the Total Channel Loss, the load admittance, Y_{load}, must be calculated that maximizes the channel gain. The maximum channel gain is given by

$$G_{\max} = \frac{1}{L}\left[1 - \left(1 - L^2\right)^{1/2}\right] \tag{42}$$

where

$$L = \frac{\left|Y_{RT}Y_{TR}\right|}{2\,\mathrm{Re}\left|Y_{TT}\right|\mathrm{Re}\left|Y_{RR}\right| - \mathrm{Re}\left|Y_{RT}Y_{TR}\right|} \tag{43}$$

5. NUMERICAL RESULTS

The performance of a communication system using identical carbon nanotube antennas is analyzed using the equations from the above sections. Results are presented using vertical dipole antennas and YAGI antennas. The antenna systems are operated in both the high GHz and at optical frequencies.

5.1 DIPOLES IN THE HIGH GHZ

Results are presented for a communication system using parallel transmit and receive carbon nanotube dipole antennas, both with half-lengths of 10 μm. Both transmit and receive antennas are assumed to be single-walled, armchair carbon nanotubes with a radius of 10 nm ($m = n = 50$). The transmitter and receiver antennas are separated in free space across a channel of length R that varies from 10 μm to 10,000 μm in distance. The transmit antenna is excited at the center of the antenna. The receive dipole is loaded at the center of the dipole. The frequency range is in the high GHz regime from 100 GHz to 1000 GHz.

In Figure 13, the normalized impedance (Z_{in} / R_o) for the carbon nanotube transmitter antenna is shown. The left and right axis of the plot is for the real part and imaginary part of the normalized impedance, respectively. The resonance of the dipole is determined when the imaginary part of the impedance crosses zero. The dipole's first resonance and anti-resonance occurs at 290 GHz and 600 GHz, respectively. These values are comparable to those results presented by Hanson's solution to Hallén's integral for the same antenna [8]. Note, for many of the calculations below, the impedance is normalized using R_o, 12,900 ohms. Again, this normalized impedance value is based on the nanoscale, dc electron transport [6].

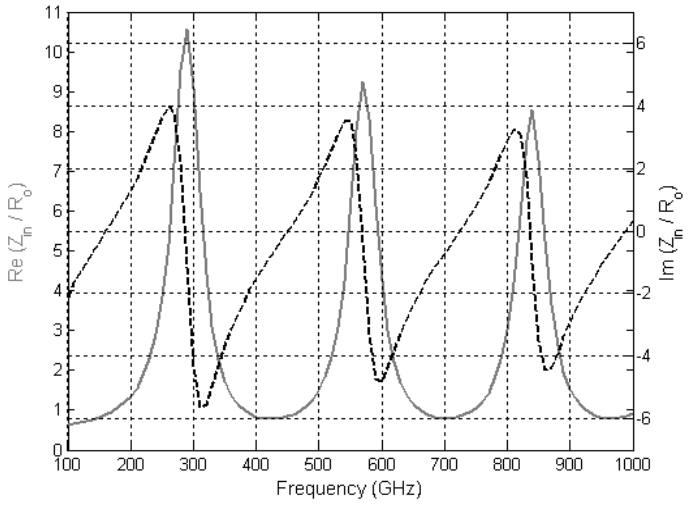

Figure 13. Normalized impedance of carbon nanotube transmitter dipole, high GHz.

Using Equation (29), the ohmic losses on the transmit antenna can be determined from the Z_S and the computed currents. In addition, the mismatch loss between the transmitter and the transmit antenna can also be determined from Equation (31). Z_T is assumed to be 12,900 ohms. Both of these results are plotted in Figure 14. The ohmic losses are considerably higher than the mismatch loss. The carbon nanotube antenna is fairly well matched to the internal impedance of a nano-transmitter with an internal impedance of 12,900 ohms. On the other hand, the high surface impedance of a carbon nanotube antenna is a significant source of power loss.

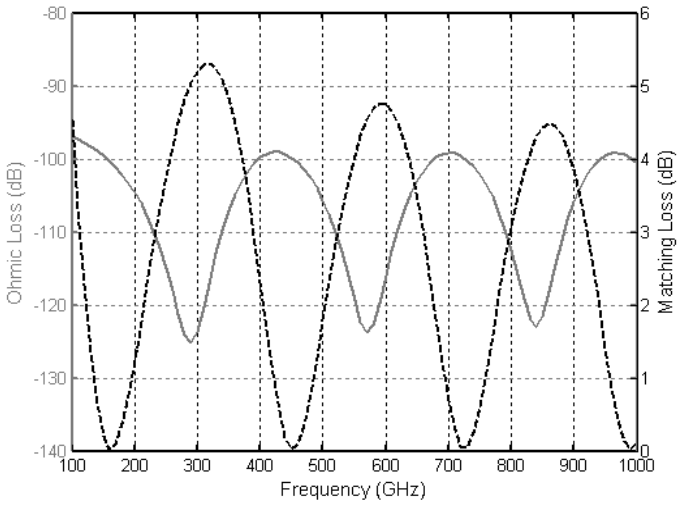

Figure 14. Ohmic and mismatch loss of carbon nanotube transmit dipole, high GHz.

Since the ohmic losses on the carbon nanotube are so high, the radiation efficiency of the antenna is expected to be very poor. In Figure 15, the efficiency for the transmit dipole antenna is plotted as a function of frequency. The dipole's efficiency has a minimum of about -93 dB at its first anti-resonance, which occurs around 600 GHz. Its maximum efficiency is at the first resonance, 290 GHz, at a calculated value of -50 dB. This means that only .000025 % of the input power is actually being radiated. Most of the input power is absorbed by ohmic loss on the carbon nanotube.

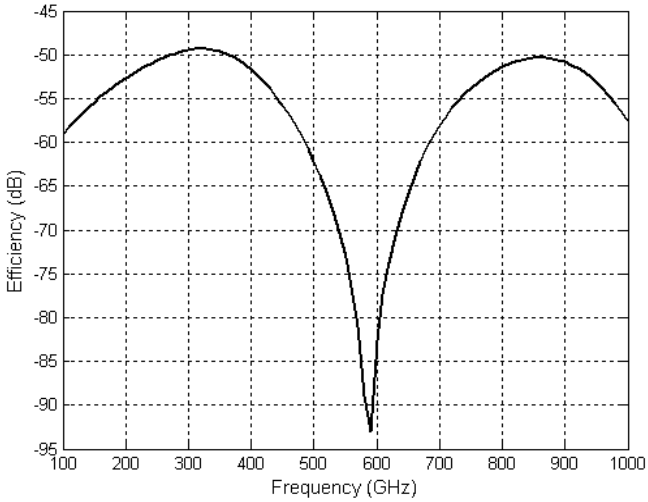

Figure 15. Efficiency of carbon nanotube transmit dipole, high GHz.

The Total Channel Loss of Equation (2) is shown in Figure 16. The transmitter and receiver are separated by distances varying from 10 μm, which is in the near field of the antenna, to 1,000 μm. At the first resonance at 290 GHz, the Total Channel Loss is nominally varying from between -50 to -150 dB as the distance between the antennas increases. Because the efficiency of the transmit antenna is so poor at its first anti-resonance of 600 GHz, there is very little power that is transmitted across the channel and the Total Channel Loss varies from between -50 to -225 dB. This Total

Channel Loss is for the optimal receiver load. However, there was minimal difference between the Total Channel Loss for the optimal receiver load and a receiver load of 12,900 ohms.

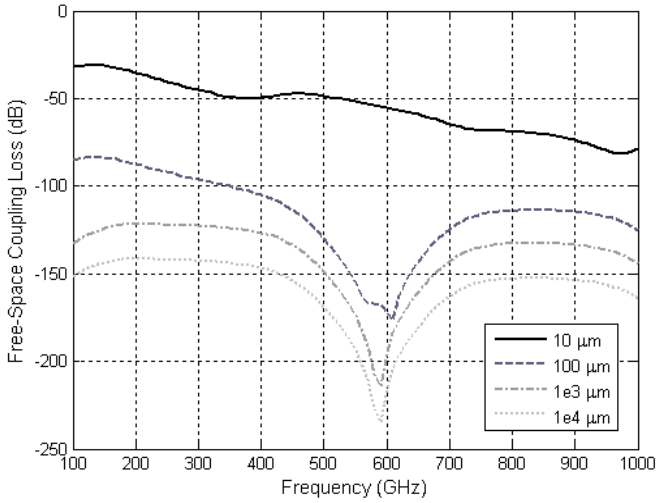

Figure 16. Total Channel Loss between transmit and receive carbon nanotube dipole antennas, high GHz.

Again, considering Equation (1), a communication link analysis is performed. For the purpose of this analysis, a Noise Figure of 7 dB is assumed. The required signal-to-noise ratio is assumed to be 5 dB. These are nominal values for the purpose of this study. Both values are optimistic for a nano-technology-based communication link. Using Equation (1), the required transmit or input power in watts can be determined for the specified parameters. The results are displayed in Figure 17. At 600 GHz and a distance of 1000 µm between the transmitter and receiver, approximately 10^5 watts of input power is required for effective communications. It is apparent that the ohmic losses severely limit the ability to effectively communication between two nanotube dipoles.

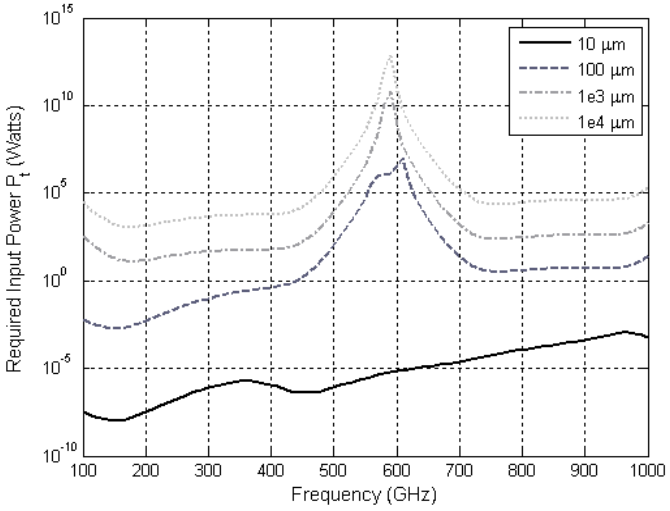

Figure 17. Required input power between transmit and receive carbon nanotube dipole antennas, high GHz.

5.2 VERTICAL DIPOLES AT OPTICAL FREQUENCIES

Results are presented for the vertically directed dipole antenna systems operating at optical frequencies (i.e., 100 THz to 800 THz). Both carbon nanotube dipole antennas have half-lengths of 150 nm with a radius of 2.72 nm ($m = n = 40$). The transmitter and receiver antennas are separated in free space across a channel of length R that varies between 100 nm to 10,000 nm in length. Again, the transmit antenna is excited at the center of the antenna. The receive dipole is loaded at the center of the dipole. Figure 18 shows the normalized impedance for the transmitting dipole antenna. At these frequencies, the dipole antenna is not resonating. The ringing in the impedance is caused by the conductivity of the carbon nanotube resonating in the optical bands.

Figure 19 shows the efficiency of the transmit dipole antenna at optical frequencies. The carbon nanotube antenna still remains very inefficient at these frequencies.

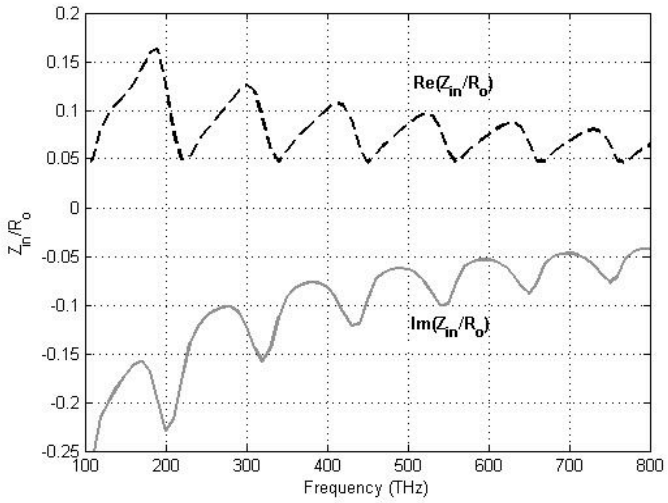

Figure 18. Normalized impedance of carbon nanotube transmit dipole, optical.

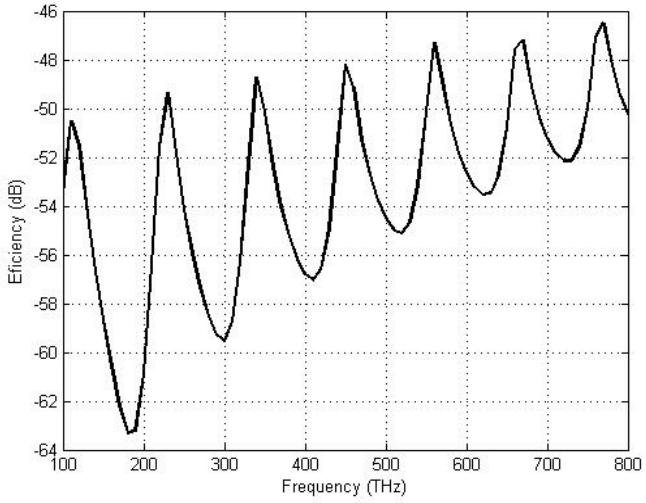

Figure 19. Efficiency of carbon nanotube transmit dipole, optical.

The Total Channel Loss is shown in Figure 20. The transmitter and receiver are separated by distances L = 100 nm, 1000 nm, and 10,000 nm. At 120 THz, the Total Channel Loss is nominally varying from between -80 to -150 dB as the distance between the antennas increases.

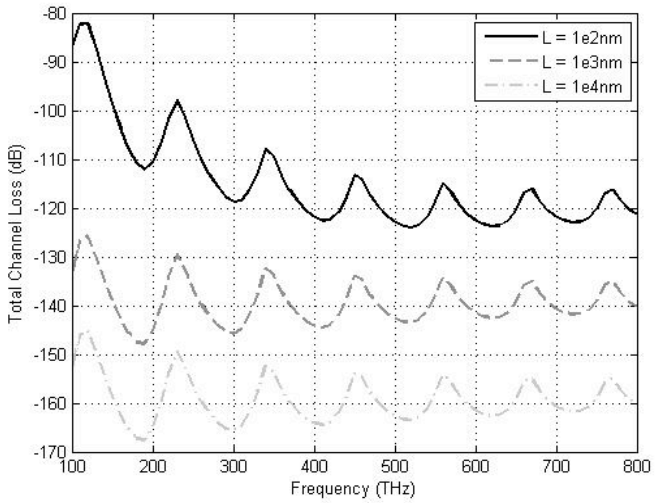

Figure 20. Total Channel Loss between transmit and receive carbon nanotube dipole antennas, optical.

5.3 ANTENNAS OF HIGHER DIRECTIVITY

A final study is performed to improve the SNR of the communication link by using antennas that would have higher directivity than the dipole antenna. As reported in [8], antennas that are considered to have higher directivity were expected to increase the magnitude of the electric field strength. YAGI antennas have higher directivity than the dipole antenna. A comparison is performed between the nanotube dipole and a three-element nanotube YAGI antenna. The specific three-element YAGI antenna would have a directive gain of approximately 9.7 dB. This would occur if the YAGI antenna is metal and operating at its first resonance.

Figure 21 shows the plotted efficiencies for the two different antennas. Surprisingly, there is very little variation between the antennas. For the two antennas, the maximum efficiency is still around 290 GHz, at a calculated value of -50 dB.

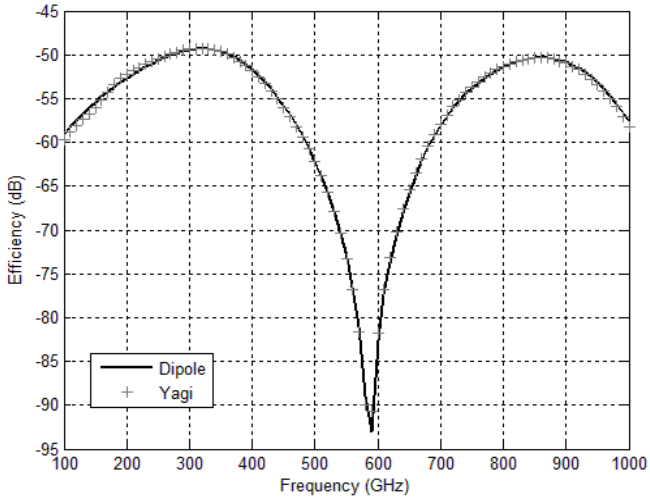

Figure 21. Efficiencies of dipole (bold) and YAGI (+)antennas, high GHz.

Finally, a communication link analysis is performed for the two antennas. The Total Channel Loss is for the optimal receiver load. Again, a noise figure of 7 dB is assumed. The required SNR is assumed to be 5 dB. The transmitter and receiver antennas are separated by distances of 100 µm, 1000 µm, and 10,000 µm. The required input power in watts for the specified parameters is shown in Figure 22. There appears to be no variation among the two antennas. It is apparent that the ohmic losses severely limit the transmitted signal. Antennas of higher directivity have limited utility in improving the communication link performance.

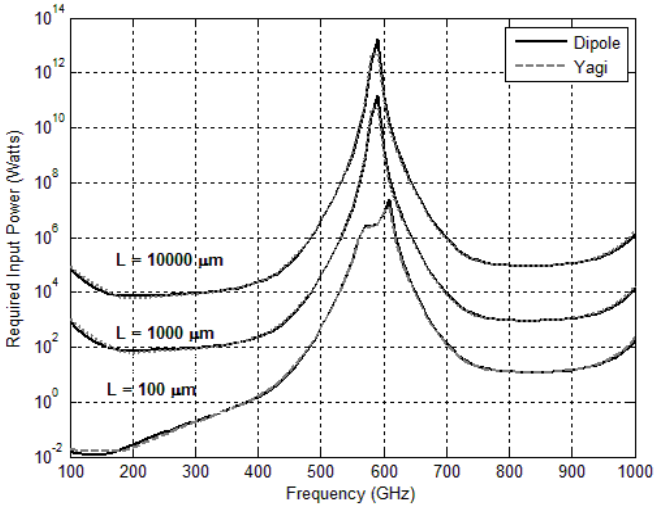

Figure 22. Required input power for dipole (bold), and YAGI (+) antennas, high GHz.

6. CONCLUSIONS

A simulation-based study has been presented for the communication link between carbon nanotube-based antennas. The approach is based on calculating a link equation given the transmitter and receiver antenna properties and losses generated in the system. Using the link equation, various feasibility studies can be performed, including estimating signal-to-noise ratios and determining minimum discernable signals. However, the focus of this study was on estimating the required input power necessary to establish a communication link given a SNR greater than zero. Because of the high ohmic losses generated on the antennas, considerable and highly improbable input power is necessary to establish the link. In order to maintain a SNR of 5 dB, input power on the order of 10 to 1e5 watts was required. While it is believed that the performance of the communication system could be further improved, it is highly unlikely that any optimized configuration could overcome the high ohmic losses.

7. REFERENCES

1. M. Bockrath, D. H. Cobden, P. L. McEuen, N. G. Chopra, A. Zettl, A. Thess, and R. E. Smalley, "Single-Electron Transport in Ropes of Carbon Nanotubes," *Science* 28, vol. 275, no. 5308, pp. 1922–1925, March 1997.
2. N. Srivastava and K. Banerjee, "Performance Analysis of Carbon Nanotube Interconnects for VLSI Applications," *ICCAD*, 2005, pp. 383–390.
3. K. Kempa, J. Rybczynski, Z. Huang, K. Gregorczyk, A. Vidan, B. Kimball, J. Carlson, G. Benham, Y. Wang, A. Herczynski, Z. F. Ren, "Carbon Nanotubes as Optical Antennae" *Advanced Materials*, vol. 19, issue 3 , pp. 421–426, Jan 2007.
4. W. Henk, C. Postma, T. Teepen, Z. Yao, M. Grifoni, and C. Dekker, "Carbon Nanotube Single-Electron Transistors at Room Temperature," *Science*, July 2001.
5. G. Slepyan, S. Maksimenko, A. Lakhtakia, O. Yevtushenko, and A. V. Gusakov, "Electrodynamics of Carbon Nanotubes: Dynamic Conductivity, Impedance Boundary Conditions, and Surface Wave Propagation," *Physical Review B*, vol. 60, pp. 17136–17149, December 1999.
6. P. J. Burke, S. Li, and Z. Yu, "Quantitative theory of Nanowire and Nanotube Antenna Performance," *IEEE Transactions on Nanotechnology*, vol. 5, pp. 314-334, July 2006.
7. Y. Lan, B. Zeng, H. Zhang, B. Chen and Z. Yang, "Simulation of Carbon Nanotube THz Antenna Arrays," *International Journal of Infrared and Millimeter Waves*, vol. 27, no. 6, June 2006.
8. G. Hanson, "Fundamental Transmitting Properties of Carbon Nanotube Antennas," *IEEE Transactions on Antennas and Propagation*, vol. 53, pp. 3426-3435, Nov. 2005.
9. J. Hao and G. Hanson, "Infrared and Optical Properties of Carbon Nanotube Dipole Antennas," IEEE Transactions on Nanotechnology, vol. 5, pp. 766–775, Nov. 2006.
10. J. Hao and G. Hanson, "Electromagnetic Scattering from Finite-Length Metallic Carbon Nanotubes in the Lower IR Bands," *Phys. Rev. B,* vol. 74, p. 035119 (1-6), 2006.
11. D. Rubin, "The Linville Method of High Frequency Transistor Amplifier Design," Naval Weapons Centre, Research Department, NWCCL TP 845, Corona Laboratories, Corona, California, March 1969.
12. R. Saito, G. Dresselhaus, and M. S. Dresselhaus, Physical Properties of Carbon Nanotubes. London, Imperial College Press, 2003.
13. R. F. Harrington, Field Computation by Moment Methods, The Macmillan Company, New York, 1968.
14. N. Champagne, D. Wilton, J. D. Rockway, **"**The Analysis of Thin Wires Using Higher Order Elements and Basis Functions," *IEEE Transactions on Antennas and Propagation*., vol. 54, no.12, Dec. 2006
15. D. Wilton and N. Champagne, "Evaluation and Integration of Thin Wire Kernels," *IEEE Transactions on Antennas and Propagation,* vol. 54, no. 4, pp. 1200–1206, 2006.
16. Junker, G. P., A. A. Kishk, and A. W. Glisson, "A Novel Delta Gap Source Model for Center Fed Cylindrical Dipoles," *IEEE Transactions on Antennas and Propagation*, vol. 43, no. 5, May 1995.
17. A. Adams, et al., "Near Fields of Wire Antenna by Matrix Methods," *IEEE Transactions on Antennas and Propagation*, vol. AP-21, No. 5, May 1973.

18. J. W Rockway and J. C. Logan, Expert MININEC Series Wire Antenna Modeling *Codes*, EM Scientific, Inc., 2000.

REPORT DOCUMENTATION PAGE

Form Approved
OMB No. 0704-01-0188

PLEASE DO NOT RETURN YOUR FORM TO THE ABOVE ADDRESS.

1. REPORT DATE *(DD-MM-YYYY)*	**2. REPORT TYPE**	**3. DATES COVERED** *(From - To)*
10–2012	Final	

4. TITLE AND SUBTITLE

FEASABILITY STUDY OF A NANO-COMMUNICATIONS LINK USING CARBON NANOTUBE ANTENNAS

5a. CONTRACT NUMBER

5b. GRANT NUMBER

5c. PROGRAM ELEMENT NUMBER

6. AUTHORS

John W. Rockway, Jeanne T. Quimby-Rockway, and John D. Rockway
SSC Pacific

5d. PROJECT NUMBER

5e. TASK NUMBER

5f. WORK UNIT NUMBER

7. PERFORMING ORGANIZATION NAME(S) AND ADDRESS(ES)

Space and Naval Warfare Systems Center Pacific (SSC Pacific)
San Diego, CA 92152–5001

8. PERFORMING ORGANIZATION REPORT NUMBER

TR 2010

9. SPONSORING/MONITORING AGENCY NAME(S) AND ADDRESS(ES)

In-house funding

10. SPONSOR/MONITOR'S ACRONYM(S)

SSC Pacific

11. SPONSOR/MONITOR'S REPORT NUMBER(S)

12. DISTRIBUTION/AVAILABILITY STATEMENT

Approved for public release; distribution is unlimited.
San Diego, California 92152-5001

13. SUPPLEMENTARY NOTES

WARNING – INFORMATION SUBJECT TO EXPORT CONTROL LAWS

14. ABSTRACT

This report details a feasibility study investigating the performance of a nano-communication system. The study is based on analyzing the suitability of carbon nanotube-based antennas to establish an effective communication link. A simulation has been developed that estimates the signal-to-noise ratio (SNR) between a carbon nanotube transmitter and its receiver separated across a free-space channel. The carbon nanotube antennas are modeled using a thin-wire approximation to the electric field integral equation and solved using the Method of Moments. In addition, the surface impedance on each wire is derived from a π-spatial tight binding model, which approximates the quantum conductive behavior of the carbon nanotube. To estimate the total channel loss, the Linville method is used to determine the power delivered from the transmit antenna to the receiver. This simulation methodology is used to perform SNR calculations for a vertical carbon nanotube dipole system in two different frequency bands (i.e., high GHz, optical). The performance of this nano-communication system is analyzed by conducting a trade-off study to determine the required input power necessary to establish an effective SNR.

15. SUBJECT TERMS

Mission Area: Net-Centric Engineering and Integration
Nano-communication system; carbon nanotube-based antennas; communication links

16. SECURITY CLASSIFICATION OF:			**17. LIMITATION OF ABSTRACT**	**18. NUMBER OF PAGES**	**19a. NAME OF RESPONSIBLE PERSON**
a. REPORT	**b. ABSTRACT**	**c. THIS PAGE**			J. D. Rockway
U	U	U	U	32	**19B. TELEPHONE NUMBER** *(Include area code)* (619) 553–5438

INITIAL DISTRIBUTION

360012	Patent Counsel	(1)
853	Archive/Stock	(1)
843	Library	(1)
853	L. Hood	(1)
56240	J. Rockway	(15)

Defense Technical Information Center
Fort Belvoir, VA 22060–6218 (1)

Approved for public release; distribution is unlimited.

SSC Pacific
San Diego, CA 92152-5001